Faraday Discussions

This paper is published as part of Faraday Discussions volume 142: Cold and Ultracold Molecules

Introductory Lecture

Papers

Discussion

Papers

Discussion

General discussion
Faraday Discuss., 2009
DOI: 10.1039/b910119p

Papers

Broadband lasers to detect and cool the vibration of cold molecules
Matthieu Viteau, Amodsen Chotia, Dimitris Sofikitis, Maria Allegrini, Nadia Bouloufa, Olivier Dulieu, Daniel Comparat and Pierre Pillet, *Faraday Discuss.*, 2009
DOI: 10.1039/b819697d

Dark state experiments with ultracold, deeply-bound triplet molecules
Florian Lang, Christoph Strauss, Klaus Winkler, Tetsu Takekoshi, Rudolf Grimm and Johannes Hecker Denschlag, *Faraday Discuss.*, 2009
DOI: 10.1039/b818964a

Precision molecular spectroscopy for ground state transfer of molecular quantum gases
Johann G. Danzl, Manfred J. Mark, Elmar Haller, Mattias Gustavsson, Nadia Bouloufa, Olivier Dulieu, Helmut Ritsch, Russell Hart and Hanns-Christoph Nägerl, *Faraday Discuss.*, 2009
DOI: 10.1039/b820542f

Rotational spectroscopy of single carbonyl sulfide molecules embedded in superfluid helium nanodroplets
Rudolf Lehnig, Paul L. Raston and Wolfgang Jäger, *Faraday Discuss.*, 2009
DOI: 10.1039/b819844f

Self-organisation and cooling of a large ensemble of particles in optical cavities
Yongkai Zhao, Weiping Lu, P. F. Barker and Guangjiong Dong, *Faraday Discuss.*, 2009
DOI: 10.1039/b818653g

Discussion

General discussion
Faraday Discuss., 2009
DOI: 10.1039/b910121g

Papers

Formation of ultracold dipolar molecules in the lowest vibrational levels by photoassociation
J. Deiglmayr, M. Repp, A. Grochola, K. Mörtlbauer, C. Glück, O. Dulieu, J. Lange, R. Wester and M. Weidemüller, *Faraday Discuss.*, 2009
DOI: 10.1039/b818391k

Ultracold polar molecules near quantum degeneracy
S. Ospelkaus, K.-K. Ni, M. H. G. de Miranda, B. Neyenhuis, D. Wang, S. Kotochigova, P. S. Julienne, D. S. Jin and J. Ye, *Faraday Discuss.*, 2009
DOI: 10.1039/b821298h

Ultracold molecules from ultracold atoms: a case study with the KRb molecule
Paul S. Julienne, *Faraday Discuss.*, 2009
DOI: 10.1039/b820917k

Two-photon coherent control of femtosecond photoassociation
Christiane P. Koch, Mamadou Ndong and Ronnie Kosloff, *Faraday Discuss.*, 2009
DOI: 10.1039/b818458e

A pump–probe study of the photoassociation of cold rubidium molecules
Jovana Petrovic, David McCabe, Duncan England, Hugo Martay, Melissa Friedman, Alexander Dicks, Emiliya Dimova and Ian Walmsley, *Faraday Discuss.*, 2009
DOI: 10.1039/b818494a

Fano profiles in two-photon photoassociation spectra
Maximilien Portier, Michèle Leduc and Claude Cohen-Tannoudji, *Faraday Discuss.*, 2009
DOI: 10.1039/b819470j

Discussion

General discussion
Faraday Discuss., 2009
DOI: 10.1039/b910122p

Concluding remarks

Concluding remarks: achievements and challenges in cold and ultracold molecules
F. A. Gianturco and M. Tacconi, *Faraday Discuss.*, 2009
DOI: 10.1039/b910178k

Sympathetic cooling by collisions with ultracold rare gas atoms, and recent progress in optical Stark deceleration

P. F. Barker,* S. M. Purcell, P. Douglas, P. Barletta, N. Coppendale, C. Maher-McWilliams and J. Tennyson

Received 28th October 2008, Accepted 5th February 2009
First published as an Advance Article on the web 28th May 2009
DOI: 10.1039/b819079h

We propose a general scheme for sympathetic cooling of molecules to μK temperatures on a timescale of seconds. Experimental parameters have been estimated from theory, which indicate the viability of the scheme. This method, which is particularly suited to optical Stark deceleration, utilises ultracold, laser cooled metastable rare gas atoms quenched to their ground state as collision partners to co-trapped molecular species within a deep optical trap (150 mK). We also describe the measurement of the role of laser-induced molecular alignment on the dipole force in optical Stark deceleration and outline progress towards the realisation of chirped optical Stark deceleration for producing slow molecular beams with mK energy spreads.

1 Introduction

Laser cooling, the cornerstone of cold atom physics, is capable of dissipatively cooling atomic gases to ultracold temperatures (μK).[1] This technique cannot, however, be applied to most molecules due to the lack of a single or even a few cycling transitions. While ultracold molecular species can be produced by association of laser cooled atomic species on Feshbach resonances[2] and by photoassociation,[3] the range of stable molecular species that can be produced in this way is limited by the small number of atomic species that can be laser cooled. New techniques have been developed to produce slow, cold molecules of much greater variety and complexity and these include buffer gas cooling,[4] and phase space filtering techniques such as electrostatic Stark deceleration[5] and more recently Zeeman deceleration.[6] These techniques are capable of producing cold trapped molecular ensembles and have now been used for a range of important low energy collision experiments[7] and precision spectroscopy.[8] However, they do not appear to be capable of reaching the ultracold regime (<1 mK), where much of the interesting physics and chemistry is to be found. To produce colder molecular gases without the losses of molecules inherent in filtering techniques, it is generally accepted that a dissipative cooling scheme will be required once the molecules are slowed and trapped using the techniques developed above. A number of important dissipative schemes are potentially available for cooling molecules below the 1 mK barrier, and these include stochastic, cavity,[9] and evaporative and sympathetic cooling.[10] Although no progress has been reported on stochastic cooling for atoms or molecules there is currently considerable theoretical effort and some experimental effort directed towards the study of cavity cooling of atoms and molecules. However, this technique is yet to be clearly demonstrated

Department of Physics and Astronomy, University College London, Gower Street, London, UK WC1E 6BT. E-mail: p.barker@ucl.ac.uk

experimentally. Evaporative and sympathetic cooling of one species *via* thermalising collisions with another colder species is conceptually simple and has been demonstrated using many cold atomic species and in a variety of traps. This method therefore appears to be a viable first choice to cool below the current 1 mK barrier. In this paper, we propose a promising route towards the sympathetic cooling of molecules which utilises ultracold, laser cooled rare gas atoms in their ground state co-trapped with molecules in an optical trap. We also describe recent developments in the optical Stark deceleration method which include the measurement of the role of laser-induced molecular alignment on the dipole force as well as progress towards the realisation of chirped optical Stark deceleration for producing slow molecular beams with mK energy spreads.

2 Sympathetic cooling with laser cooled rare gas atoms

The earliest sympathetic cooling experiments with stable cold molecules were carried out with helium gas.[4] This technique, called buffer gas cooling, uses collisions between helium gas at temperatures in the 100 mK range with paramagnetic molecular species, which are accumulated in a magnetic trap as they are cooled. This method has proven to be very successful for a number of molecular species but it is currently limited to temperatures in the 100 mK range. Sympathetic cooling of Stark decelerated species with laser cooled atoms is also a potential route towards μK temperatures. The collisional properties of a few molecular species, which can be subsequently electrostatically or magnetically trapped with laser cooled alkali metal atoms have been explored theoretically.[11,12] These studies show that maintaining a large elastic to inelastic collision ratio of rates is problematic over all of the temperature ranges in which the molecules must be sympathetically cooled. Molecules that can be electrostatically and magnetically trapped in a single quantum state can experience trap losses when inelastic collisions promote them to untrappable states. In addition, chemical reactions between the species can also lead to an effective trap loss.[12] We propose a scheme for sympathetic cooling of optical Stark decelerated molecules using ground state rare gas atoms as collision partners to minimise the possibility of reactions and avoid losses due to state changing collisions. An optical trap is an obvious choice of trap for sympathetic cooling experiments, since it is capable of trapping all ro-vibrational states in the electronic ground state, unlike magnetic and electrostatic traps. However, in order to make a trap deep enough to hold optical Stark decelerated molecules in the 10–100 mK range, it must have a small volume with length scales of the order of a hundred microns. This type of small volume trap does not, at first, appear attractive for electrostatic Stark and Zeeman deceleration techniques, which produce slowed single quantum state densities in the 10^8 cm^{-3} range over millimeter length scales, as very few molecules would be trapped. It does, however, appear to be a feasible method for trapping optical Stark decelerated molecules with densities in the 10^{12} cm^{-3} range, because the optical lattice used in these experiments is spatially well matched to optical trap dimensions. In addition, an optical trap is capable of trapping a molecular gas that is in a distribution of ro-vibrational states and these internal states may also be cooled using evaporative and sympathetic cooling within the trap.

2.1 State preparation for trapping and sympathetic cooling

Optical cooling of five rare gas atoms has been achieved by utilizing a closed transition from the lowest excited meta-stable state $ns[3/2]_2$ to the higher $np[5/2]_3$ state.[13–17] We have considered viable optical quenching routes for He, Ne, Ar, Kr and Xe, from the meta-stable 'cooling' states with special consideration given to the heating effect caused by the absorption of near infra-red photons and emission of VUV photons in the quenching process. Quenching of Ne*, Ar*, Kr* and Xe* can be achieved by optically pumping from the meta-stable state to a higher energy state

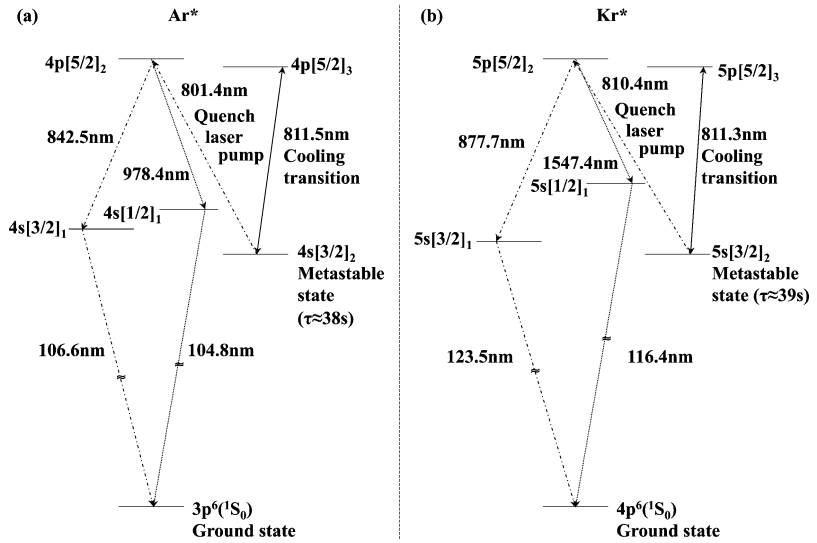

Fig. 1 Energy levels relevant for laser cooling and quenching of Ar* and Kr*.

which can undergo one or more dipole transitions to the ground state. Two such routes for Ar* and Kr* are illustrated in Fig. 1.

Argon can be optically quenched by pumping from the $4s[3/2]_2$ meta-stable level to the $4p[5/2]_2$ excited state using light at 801.4 nm. There are two possible two-photon decay routes from the $4p[5/2]_2$ level to the ground state; the intermediate levels are $4s[3/2]_1$ and $4s[1/2]_1$. This quenching process will give a maximum photon recoil temperature of 66 μK. A laser of wavelength 763.5 nm could also be used in an alternative quenching process exciting the $4p[3/2]_2$ state from which the atom could decay to the ground state *via* the same two intermediate levels as in the previous process. A maximum temperature increase of 68 μK will result from the photon recoil effect.

The quenching scheme for krypton is similar to that for argon; the $5s[3/2]_2$ meta-stable state is optically pumped, by 810.4 nm light, to the $5p[5/2]_2$ state from which dipole transitions to the ground state can proceed *via* either the $5s[3/2]_1$ or $5s[1/2]_1$ states. This process will produce a temperature increase of 25 μK. Laser light at 760.2 nm can also be used to quench Kr* by pumping to the $5p[3/2]_2$ state from which decays to the ground state result in a heating effect of 25 μK. Ne* and Xe* can be quenched using laser light at 633.4 nm and 979.9 nm respectively. The quenching process heats Ne by 261 μK and the heavier Xe by 11 μK.

We note that it is not possible to quench He* in the same way but this may be achieved by other methods.[18] However, the atomic cloud will be heated by more than 1.2 mK, due to the emission of a short wavelength ($\lambda < 64.5$ nm), high energy photon and thus He from this perspective appears to be an unsuitable species for sympathetic cooling.

2.2 A deep optical trap for molecules and rare gas atoms

Although the ultracold atomic species can easily be trapped in conventional quasi-electrostatic traps (QUEST),[19] one of the primary challenges is to create a continuous optical trap that is sufficiently deep to trap the initially 'hot' molecular species. To create the necessary trap depth we consider an optical potential that can be created within a high finesse optical buildup cavity.[20–22] For frequencies far-detuned (to the red) from any possible dipole-allowed transitions, a QUEST standing wave potential takes the general form

$$U(x,y,z) = -\frac{\alpha}{2}E(x,y,z)^2, \quad (1)$$

where α is the ground state polarizability of the trapped particle, and $E(x,y,z)$ is the electric field distribution of an incident light field. In the specific case of a Gaussian beam in-coupled to a Fabry–Perot buildup cavity, a stationary periodic lattice potential is formed, which can be described by

$$U(r,z) = \frac{U_0}{1+(z/z_R)^2}\exp\left[-2(r/w(z))^2\right]\cos^2[kz], \quad (2)$$

where $U_0 = \frac{2\alpha}{\varepsilon_0 c} I_c$, I_c is the one-way circulating peak intensity, z_R is the Rayleigh range of the intra-cavity field ($z_R = \pi w_0^2/\lambda$), w is the $1/e^2$ beam width in the radial direction, and $k = 2\pi/\lambda$. U_0 signifies the peak well depth. The beam waist evolves according to $w(z) = w_0[1 + (z/z_R)^2]^{1/2}$, where w_0 is the minimum beam waist at the cavity centre. A plot of the intra-cavity potential is given in Fig. 2. The variation in potential well depth for a QUEST is determined by the difference in polarizability of each species.

2.3 Cavity design

We describe a prototypical optical trap with a well depth of 150 mK for benzene molecules which requires a circulating intensity of $I_c = 2.5 \times 10^8$ W cm^{-2}. We consider a trap that could be constructed from a commercial, single frequency laser of 10 W output power (Verdi V10, Coherent), operating at a wavelength of 532 nm fed into an optical buildup cavity. In such a scheme it is possible that 65% of the initial laser power would be lost before it is coupled into the cavity. Damage to the mirror surfaces due to the high intra-cavity intensity necessitates a minimum beam spot size on the mirrors such that the intensity is below $\sim$ 100 MW cm^{-2}.[23] This leads to a minimum beam waist radius in the trapping region of the cavity of $w_0 = 55$ μm. This beam waist must also be sufficient to overlap well with our optical Stark deceleration volume so that the total number of trapped molecules is maximised. To produce the required intensity of $I_c = 2.5 \times 10^8$ W cm^{-2}, we consider

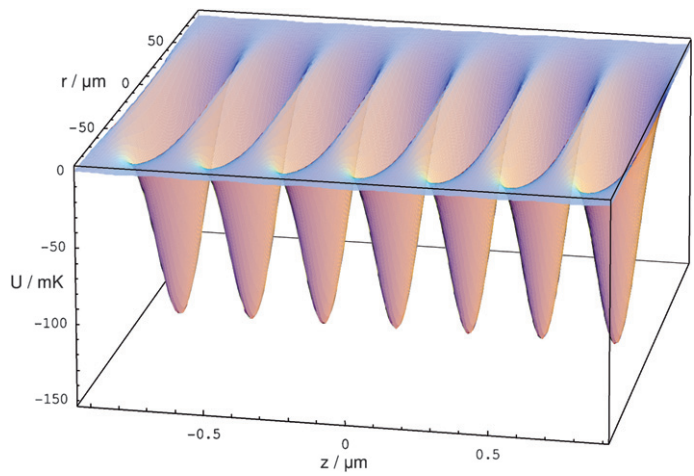

Fig. 2 A plot of the intra-cavity trapping potential for benzene molecules within the high finesse cavity.

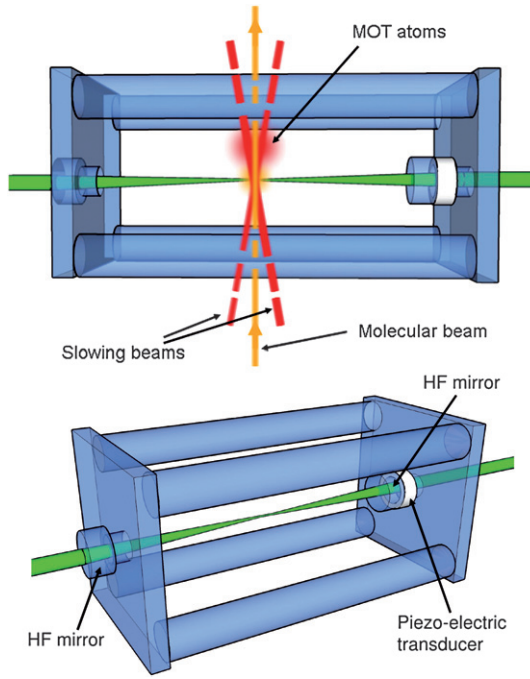

Fig. 3 Fused-silica cavity design. Molecular slowing beams are shown in red, intersecting at the beam waist of the 532 nm (green) dipole trap beam at the centre of the cavity (the trapping point).

a cavity consisting of two, high-reflectivity mirrors (radius of curvature $R = 5$ cm) which share the same optical axis, separated by a distance $L = 8.5$ cm. Fig. 3 is a diagram of the buildup cavity trap suitable for trapping optical Stark decelerated molecules. The mirrors are assumed to be supported on a structure made of a low thermal expansion material such as fused silica, but with optical access for the lattice deceleration beams and for the magneto-optical trap. The mirror transmission coefficients T must be chosen to enable a sufficiently large power build-up inside the cavity to produce the required intensity. For a perfectly impedance-matched cavity, the in-coupling mirror has transmissivity T_1 given by

$$T_1 = \frac{1}{G} = \frac{P_c}{P_I}, \tag{3}$$

where G is the cavity power build-up factor, P_c is the intra-cavity intensity (one-way), and P_I is the in-coupled laser power. The impedance matching condition fixes the in-coupling mirror transmission coefficient: $T_1 = T_2 + L$, where T_2 is the transmission coefficient of the second mirror, and L is the total loss coefficient for the cavity. This condition maximizes the power build-up. A one-way intra-cavity intensity of $I_c = 2.5 \times 10^{12}$ W m^{-2} gives a well depth of $U_0 = 150$ mK for benzene. With $w_0 = 55$ μm we obtained $P_c = 23.5 \times 10^3$ W, hence the required transmission coefficient is $T_1 = 149$ parts per million (ppm). Assuming realistic loss coefficients of 10 ppm for each mirror, we then find $T_2 = 129$ ppm. Using these values we calculate a suitable cavity's required spectral properties. These are a finesse of $F = 19800$, a free spectral range $FSR = 1.76$ GHz and a linewidth of $\Delta\nu = 89.3$ KHz, and the power buildup of $G = 6710$. All of these values have been achieved in many high finesse cavities[20–22] and therefore we conclude deep molecular traps constructed in this way are feasible.

We note that laser frequency instabilities, as well as thermal and vibrational instability in the cavity all lead to difficulties in maintaining a stable, single intra-cavity mode. For our purposes, a TEM_{00} Gaussian mode is preferable for the formation of a deep QUEST trap. Therefore, to avoid higher order TEM-modes forming, the cavity length and/or laser frequency have to be actively stabilized using standard Pound–Drever–Hall techniques.[24,25]

2.4 Dipole trap potential for rare gas atoms and optical Stark decelerated molecules

The QUEST produces different well trap depths for each of the possible rare gas atoms and molecules due to their differing static polarizabilities. Table 1 shows the corresponding well depth U_0 for a one-way intra-cavity intensity of $I_c = 2.5 \times 10^8$ W cm^{-2}.

These well depths are compared with the temperature of the atoms after laser cooling and quenching to their ground state, since this has to be much lower (10×) than U_0 for sympathetic cooling to be effective.[20]

To estimate the number of molecules loaded into the lattice/dipole trap potential sites we assume that the molecular beam has a uniform density of $\rho = 10^{13}$ cm^{-3}, and that the volume of a lattice potential site is $V_{LS} = \pi w_0^2 \times a = 2.53 \times 10^{-9}$ cm^3, where a is the axial lattice spacing ($a = 0.266$ μm). Because of the small solid angle subtended by the lattice deceleration beam the transverse temperature ($T_x = T_y$) of benzene in a molecular beam is approximately 400 μK at 0.2 m from the orifice, while the longitudinal temperature T_z is approximately 1 K. The total number of molecules trapped in our lattice potential per lattice site thus depends on the density of the beam, the size of a potential site and also the proportion of the velocity distribution of molecules that can be captured by a potential depth of around 150 mK (for benzene). To simplify the calculation, we assume 100% trapping in the transverse direction (reasonable since $T_{x,y} \ll U_0$), and therefore model the beam as having a 1D velocity distribution given by $f(v_z) = \left(\frac{m}{2\pi k_B T_z}\right) \exp\left[-\frac{m v_z^2}{2 k_B T_z}\right]$, where m is the molecular mass, and v_z is the axial velocity of a constituent molecule in the distribution. During the confinement process, evaporative cooling takes place, which rejects all molecules with temperatures approximately above 1/10th of the potential depth ($T > 15$ mK). The fraction, n, of molecules captured by the trap is given by

$$n = \int_{-v_z(T=15\text{ mK})}^{v_z(T=15\text{ mK})} \left(\frac{m}{2\pi k_B T_z}\right) \exp\left[-\frac{m v_z^2}{2 k_B T_z}\right] dv_z, \quad (4)$$

where $v_z(T = 15\text{ mK}) = 1.26$ m s^{-1}, and $n = 0.097$. The total number of molecules trapped per lattice site is then $N_{LS} = \rho \times V_{LS} \times n = 2450$. With a molecular beam width of ≈ 100 μm, this gives a total number for the whole lattice of 0.92×10^6 molecules. Using the same arguments we would expect that 700 H_2 molecules could be trapped in each lattice site and used as a starting point for sympathetic cooling. This model neglects loss mechanisms that may be present during loading, and

Table 1 The calculated well depth for each rare gas species and the recoil temperature after quenching to its ground state

Rare gas	U_0/mK	Recoil temp./μK
He	3.08	1216.0
Ne	5.95	261.1
Ar	24.7	66.3
Kr	37.4	24.8
Xe	60.8	11.1

assumes a high value for the molecular beam density. This number is therefore an upper limit. Although we have considered benzene in these calculations the well depth for any species can be scaled by its polarizability. The well depths for H_2, NH_3 and CS_2 are 12 mK, 33 mK and 127 mK respectively.

2.5 A case study: sympathetic cooling of molecular hydrogen

Molecular hydrogen is an interesting first species to consider for sympathetic cooling since it is of astrophysical importance and is a candidate for ultracold chemistry experiments. Its collisional properties, in the absence of a trapping field, can be readily calculated, and it has a high polarizability to mass ratio which means that it is one of the most effective species to decelerate using optical Stark deceleration.[26,27] In order to estimate thermalisation times in the optical trap it is necessary to determine scattering lengths and collision cross sections for collisions between the rare gas atoms and the molecules of interest. Cold and ultracold calculations of cross sections for H_2 with He and Ar have been already considered in some detail[28,29] and we have extended these to include all the stable rare gas atoms that can be laser cooled and trapped.[30,31] H_2 is a simple first case to consider as the scattering energy is very small compared to the vibrational–rotational excitation energies of H_2, and thus the only allowed channel is the elastic one. Under these conditions, the scattering of Rg–H_2 was modelled as a two-body process.[32,31]

Table 2 shows the range of values obtained for the Rg–H_2 scattering length and the cross section. The spread in these values for all species except Xe–H_2 results from the variation in the published potential energy surfaces (PES).[31] For Xe–H_2, there is only one PES reported. The table illustrates that although there are large uncertainties in the collisional parameters, the physics of the scattering mechanisms is clear. The greatest cross-section is of He–H_2, due to the strong halo characteristics of this system.[33,32] It is possible to show that for those systems the scattering length, a_s depends on the square root of the inverse of the binding energy E, $a_s \approx 1/\sqrt{E}$. The smaller the binding energy the larger the scattering length and the five complexes can be interpreted in this way. The two He–H_2 isotopologues are the weakest bound and their scattering length is the greatest while the Ne–H_2 system is more strongly bound and its scattering length is smaller. The stabilization of a second vibrational band in Ar–H_2 makes this complex more reactive than its predecessor and the Xe–H_2 scattering length is the smallest of the whole group.

The large collisional cross-sections for ^{4}He–H_2 and Ar–H_2 are comparable to that utilized in sympathetic cooling experiments between cold alkalis[10] and these values are relatively constant over a large temperature range. We estimate a collision rate and thermalisation time for Ar–H_2 based on a cross-section of 1000 Å^2 and the axial and radial trap frequencies, assuming the harmonic approximation given as $\omega_{ax} = \sqrt{2\frac{U_0 k^2}{m}}$ and $\omega_{rad} = \sqrt{4\frac{U_0}{mw^2}}$ respectively. The radial and axial trap frequencies for Ar are $2\pi \times 15$ kHz and $2\pi \times 7$ MHz and for H_2 are $2\pi \times 41$ kHz and

Table 2 The scattering lengths a_s and the zero-energy elastic cross-sections σ calculated for all Rg–H_2 complexes

	$\lvert a_s \rvert$/Å	$\sigma(E = 0)$/Å^2
^{3}He–H_2	67.6–90.6	57500–103000
^{4}He–H_2	22.7–24.7	6500–7800
Ne–H_2	3.30–3.85	140–190
Ar–H_2	8.71–10.1	950–1300
Kr–H_2	5.51–6.96	380–610
Xe–H_2	1.82	42

$2\pi \times 19$ MHz. We also assume that H_2 has evaporated to approximately one tenth of the well depth before sympathetic cooling occurs. We assume that each species has a density in the trap of the form $n = n_0 \exp[-U/kT]$ with peak densities of 5×10^9 cm^{-3} and 10^{11} cm^{-3} corresponding to 11 molecules and 1300 atoms per fringe of the trap at initial temperatures of 1.2 mK and 66 μK respectively. The Rg–H_2 collision rate is given by $\gamma = \sigma v_{\mathrm{rel}} \int n_{\mathrm{Rg}}(\mathbf{x}) n_{\mathrm{H_2}}(\mathbf{x}) \mathrm{d}\mathbf{x}$, v_{rel} is the mean relative velocity between collision partners and $n_{\mathrm{Rg}}(\mathbf{x})$ and $n_{\mathrm{H_2}}(\mathbf{x})$ are the densities of the rare gas and H_2. It is well known that approximately 3 collisions are required for thermalisation of collision partners of equal mass in a gas but for unequal masses this is approximated by $\frac{3}{\eta}$ where $\eta = 4\frac{m_{\mathrm{Rg}} m_{\mathrm{H_2}}}{(m_{\mathrm{Rg}} + m_{\mathrm{H_2}})^2}$. The initial time for thermalisation for two species within a trap is given by[10]

$$\tau = \frac{3\pi^2 k_{\mathrm{b}} T_{\mathrm{H_2}}}{\left(N_{\mathrm{H_2}} + N_{\mathrm{Rg}}\right)\sigma\eta m_{\mathrm{H_2}} \omega_{z\mathrm{H_2}} \omega_{r\mathrm{H_2}}^2}. \tag{5}$$

For the conditions given for Ar–H_2, a thermalisation time scale of 2 ms is determined. This fast thermalisation time can be accounted for by the large axial trap frequency and the large relative velocity between the hot molecular gas and the much colder atoms, despite the poor spatial overlap between the two species. For Xe–H_2 collisions, using the same initial densities and a collision cross-section of 42 $Å^2$, a thermalisation time of the order of seconds is estimated. Although the Xe–H_2 collision rate is much lower than for Ar–H_2, trapping of atomic species over this time scale has been demonstrated indicating that even Xe, which forms the deepest trap, could be used for sympathetic cooling.

3 Measuring the effect of molecular alignment on the dipole force

The optical dipole force on a ground state atomic species in a QUEST is proportional to isotropic polarizability. The force on molecules however, has an orientational dependence due to their non-spherical shape and anisotropic polarizability. In the relatively low intensity field of the QUEST described above, the rotational motion of a molecule averages to its static value. However, in the strong non-resonant laser fields (10^{11} W cm^{-2}) that are used to decelerate molecular species in optical Stark deceleration, molecules can be aligned with respect to the polarization of the field. For a molecule irradiated by a non-resonant pulsed optical field with an electric field of the form, $\mathbf{E}(r,t) = \frac{1}{2}\hat{\varepsilon}E(r,t)\exp^{i\omega l t} + c.c.$, where $\hat{\varepsilon}$ is a unit vector of the field polarization, $E(r,t)$ is its amplitude and ω_l its frequency, the induced dipole potential or Stark shift is given by[34,35]

$$V(t) = -\frac{1}{4}\alpha_{\mathrm{eff}} E(r,t)^2. \tag{6}$$

The effective polarizability and the optical Stark potential are dependent on the amplitude of the laser field and its polarization. For linearly polarized light incident on a linear or symmetric top molecule, the effective polarizability is given by[36] $\alpha_{\mathrm{eff}} = [\Delta\alpha\cos^2\theta + \alpha_\perp]$, where $\Delta\alpha = \alpha_\parallel - \alpha_\perp$ and $\alpha_\parallel$ and $\alpha_\perp$ are the parallel and perpendicular polarizabilities with respect to the molecular symmetry axis. For a linear molecule the symmetry axis is along the bond axis as shown in Fig. 4. For linearly polarized light the polarization vector is perpendicular to the direction of the light field and θ is the angle between the symmetry axis and the polarization direction as shown in Fig. 4a. For circularly polarized light, whose polarization is in a plane orthogonal to the propagation direction, the angle θ is between the symmetry axis and the propagation direction as shown in Fig. 4b. The effective polarizability is $\alpha_{\mathrm{eff}} = \frac{1}{2}[\alpha_\perp + \alpha_\parallel - \Delta\alpha\cos^2\theta]$. These alignment-dependent optical potentials produce

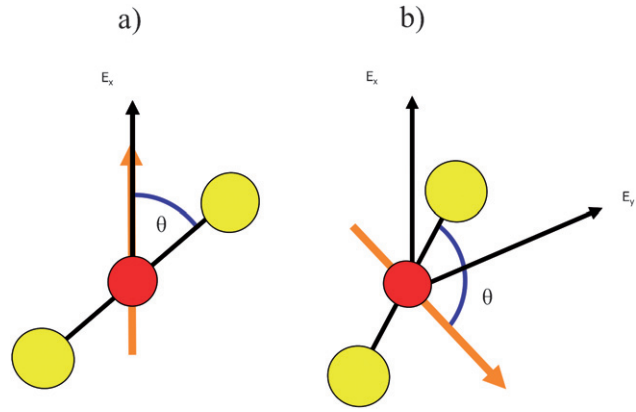

Fig. 4 The orientation of the linear molecule CS_2 with respect to the polarization vector for linearly and circularly polarized light defined by the angle θ.

a centre-of-mass force that is proportional to the gradient of the potential, $\mathbf{F} = -\boldsymbol{\nabla} V(r,t)$, which acts to push molecules into the higher field regions of an optical field. For linearly polarized fields the maximum force is determined by the maximum effective polarizability which occurs when $\cos^2\theta = 1$ and the molecule is exactly aligned with the polarization vector leading to $\alpha_{\text{eff}} = \alpha_{\|}$. For circularly polarized light, the maximum polarizability occurs when $\cos^2\theta = 0$ and the molecule moves in the plane orthogonal to the polarization vector. These values will be less than these maximum values and this can be determined from the expectation value of $\cos^2\theta$ for a particular laser intensity and polarization by solution to the Schrödinger equation for a rigid rotor perturbed by the optical Stark potential. The aligned molecular wavefunction, $\Psi(t) = \sum_{JM} C_{J,M}(t)|JM\rangle$, is a superposition of the field free rotor wave-functions[37] $|JM\rangle$, where J are the quantum numbers for angular

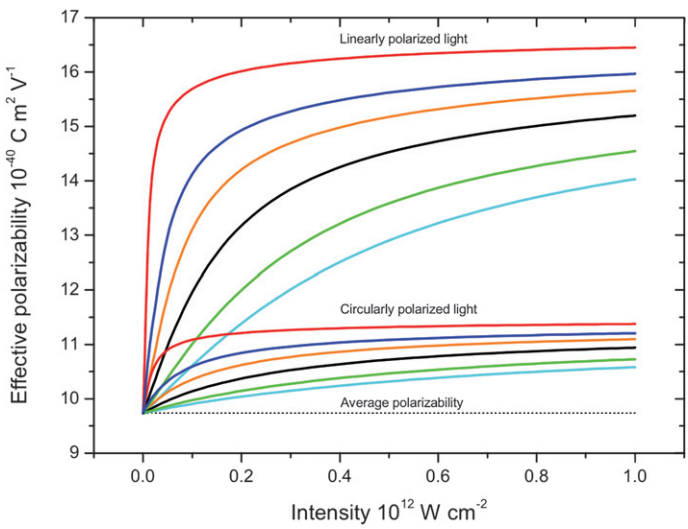

Fig. 5 The effective polarizability is plotted against the nonresonant laser intensity for rotational temperatures 2 K (red), 4 K (dark blue), 6 K (orange), 8 K (black), 10 K (green), 12 K (light blue), for linearly polarized light and circularly polarized light. The average polarizability is also shown for comparison (dashed line).

momentum and M is its projection onto a space-fixed axis. For a particular polarization and laser intensity an expectation value[38] of $\langle\cos^2\theta\rangle_{J,M}(t)$ can be determined and averaged according to an initial population distribution allowing a calculation of the effective polarizability as a function of laser intensity and rotational temperature. These values for both circular and linear polarization are plotted as a function of intensity for CS_2 in Fig. 5. The static polarizabilities of CS_2 are $\alpha_{\parallel} = 16.8 \times 10^{-40}$ C m^2 V^{-1} and $\alpha_{\perp} = 6.2 \times 10^{-40}$ C m^2 V^{-1} and the rotational constant is $B = 0.109$ cm^{-1}. Fig. 5 shows that the effective polarizability is higher for linear polarization and that all values saturate at higher intensities.

To measure the effect of molecular alignment on the dipole force we have measured the induced velocity imparted to carbon disulfide molecules in a cold molecular beam by an optical field of nanosecond duration and intensity in the 10^{12} W cm^{-2} range. This setup has been described elsewhere[35] and so we only briefly summarize it here. A cold molecular beam of carbon disulfide is formed by expanding CS_2 gas diluted in argon through a pulsed solenoid valve into a vacuum chamber. The centre of the molecular beam passes through an orifice (skimmer) and enters a second differentially pumped vacuum chamber at a pressure of 10^{-7} torr. The translational temperature of the beam is 2.1 K, travelling at an average velocity of 520 ms^{-1}. The molecules pass into a time-of-flight mass spectrometer, where they intersect a non-resonant infra-red (IR) optical field of wavelength 1064 nm, which induces a dipole force on the molecules. The focus of the optical field has a Gaussian spatial profile with an e^{-2} radius of 20 μm and Rayleigh range (constant spot diameter along the propagation direction) of 300 microns with a peak intensity of 6×10^{11} W cm^{-2}. The focusing lens is mounted on an XYZ translational stage outside the vacuum chamber which can position the beam with a resolution of ±1 μm. The single frequency IR laser beam is created by an injection seeded, Q-switched Nd:YAG laser which produces a temporally smooth intensity profile for the duration of the 15 ns pulse. The IR beam initially has a linear polarization of better than 1 part in 10^4 by passing it through two thin film polarizers. When required, the field polarization is converted to near circular polarization at the same intensity by passing the light through a $\frac{\lambda}{4}$ zero order wave-plate. To measure the velocity imparted to the molecules by the dipole force from the IR field we ionize the neutral molecules once the IR field is turned off. The velocity of the neutrals is measured in a Wiley-Maclaren time-of-flight mass spectrometer by converting the change in time-of-flight (TOF) to a change in velocity. Detection of the molecules is accomplished by ionization of the molecules after the IR field is applied using a (3 + 1) resonance enhanced multiple photon ionization (REMPI) scheme *via* the three photon transition $[\frac{1}{2}]np\sigma_u(^1\Pi_u) \leftarrow X^1\Sigma_g^+$.[39,40] Using a peak intensity of $7.6 \pm 2.3 \times 10^{11}$ W cm^{-2} for the linearly polarized light and $7.1 \pm 2.1 \times 10^{11}$ W cm^{-2} for near circular polarization we measure the variation in the dipole force measured at different locations across the center of the focused IR beam along the direction of the molecular beam. The measurements are made by alternating between both types of polarization by rotation of the waveplate so that the measurement is always taken at same position with respect to the IR beam. Velocity changes in this direction are either due to acceleration or deceleration of the molecules due to the dipole force. These measurements were made for both linear and circular polarization and each data point corresponds to a 1200 shot average of the TOF spectrum with the probe beam at different spatial positions across the IR beam. A typical TOF spectra for each polarization is shown in Fig. 6 where the intensity gradient of the IR beam is highest. For comparison the unperturbed TOF, where no IR beam is present, is also shown. By averaging a number of these measurements we find that the TOF and thus the velocity imparted to molecules changes by 25%. This occurs when changing from linearly to circularly polarized when the laser intensity for each case only changes by 6%. These results indicate that the change in the velocity shifts and thus the dipole force is due to field induced alignment. This difference is

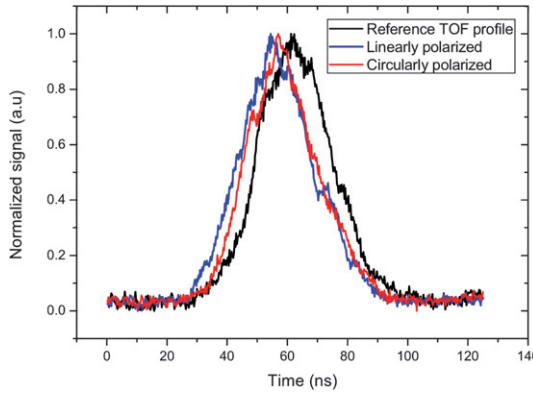

Fig. 6 Time-of-flight (TOF) spectra of CS_2 in the molecular beam when perturbed by a linearly and circularly polarized field as well as the unperturbed reference TOF when the field is turned off.

based on the peak velocity shifts of approximately 10 ms^{-1} for linearly polarized light and 7 ms^{-1} for circularly polarized light (Table 3). To compare our results with that predicted from field induced alignment we calculate the velocity changes due to both polarizations for rotational temperatures from 2 to 12 K. The velocity imparted to the molecules *via* the dipole force is determined by numerically solving the classical equation of motion of a molecule in the optical field from $F = m\frac{d^2x}{dt^2} = -\nabla V$ for the experimental conditions described above. The intensity of the laser field can be related to electric field by $I = \frac{\varepsilon_0 c}{2}E^2$. For the near impulsive kick to the center-of-mass motion, induced by the 15 ns duration of the laser, the induced velocity change is directly proportional to intensity and effective polarizability and we find that the differences in velocity do not strongly depend on temperatures above 8 K. As the uncertainty in the intensity is 30%, we find a best fit to the measured velocity shifts by allowing the intensity to vary within its uncertainty determined by experiment. Our best fit for both polarizations gives an intensity of 6.0×10^{11} W cm^{-2} for the linear case and 5.6×10^{11} W cm^{-2} for the circularly polarized case. The variation between these two values is approximately 6%, consistent with the variation in intensity between these two polarizations. Using this peak intensity and a rotational temperature of 12 K we obtain a maximum effective polarizability of 13.2×10^{-40} C m^2 V^{-1} for the linear case and 10.4×10^{-40} C m^2 V^{-1} for the circularly polarized case, with $\langle\cos^2\theta\rangle = 0.66$ for linearly and $\langle\cos^2\theta\rangle = 0.21$ for circularly polarized light. The average polarizability of a linear molecule that is not aligned by the field is 9.7×10^{-40} C m^2 V^{-1}. The field free alignment expectation value $\langle\cos^2\theta\rangle$ is equal to $\frac{1}{3}$. The well depths for the linearly polarized beam are $U/k_b = 72$ K for linearly and $U/k_b = 57$ K for circularly polarized light.

Table 3 The measured peak velocity changes of CS_2 molecules accelerated and decelerated by the dipole force from a focused Gaussian beam, for different polarizations. The peak velocity changes occur where the focused beam has the highest intensity gradient

	Lin. Pol.	Circ. Pol.	Difference
Acceleration	9.9 ± 0.6	6.4 ± 0.5	3.5 ± 0.8
Deceleration	-9.9 ± 0.5	-7.2 ± 0.3	2.8 ± 0.6

The ability to control the effective polarizability *via* field polarization allows us to tailor the optical well depth and thus optical Stark deceleration. Of perhaps even more importance is that the effective polarizability is dependent on rotational state when strong fields are used. This may allow the use of these fields for spatial state selection of different rotational states when using a single focused beam before optical Stark deceleration. Such separation may be important in evaporative and sympathetic cooling where thermalisation of molecules in higher rotational states will act to heat molecules trapped in an optical trap.

4 Progress towards chirped deceleration experiments

Optical Stark deceleration is a phase space filtering technique which traps and decelerates cold molecules produced in a molecular beam and brings them to rest. In this typically two stage process the molecules are initially cooled by collisions with rare gas atoms in a supersonic expansion and reach temperatures in the 1 K range. The cold molecules in the molecular beam are, however, accelerated to supersonic speeds, and therefore a second stage is required to trap and transport some part of this initial phase space distribution, centered at the velocity of the molecular beam, back to the laboratory frame. In optical Stark deceleration the potential is created by an interaction between an induced dipole moment and the intense optical field that induced it. Since all molecules can be polarized in this way, in principle, any molecule or atom can be manipulated and slowed in the same manner. This capability has been demonstrated in previous experiments, where molecules were slowed using a moving lattice potential utilising a half phase space rotation or half oscillation in the lattice to rapidly decelerate or accelerate molecules.[26,27] This technique has been shown to produce a slowed distribution with a minimum energy spread that is at best equal to the initial energy distribution of the molecular beam. Although this is acceptable for loading a trap, because a narrower energy distribution can be achieved in a shallower trap, it is not suitable for a range of collision experiments where a narrow energy distribution is required. In addition, very fast switching of the optical fields is required. The creation of slowed energy distributions that are narrower than the molecular beam have been studied theoretically using chirped optical Stark deceleration.[41] This scheme uses a lattice that is initially

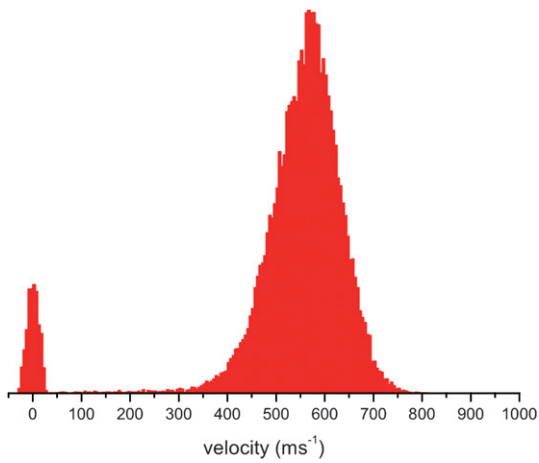

Fig. 7 Simulated velocity distribution function after chirped deceleration of H_2 seeded into a molecular beam with an initial temperature of Ar at 560 K with a FWHM energy spread of 70 mK. The laser is chirped over 1.1 GHz in 150 ns and requires an energy of 60 mJ per lattice beam.

travelling at the molecular beam velocity and traps a narrow energy distribution determined by the well depth of the potential. The lattice is constantly decelerated to zero velocity, transporting a fraction of the cold molecules to zero velocity in the laboratory frame. In practice the decelerating lattice is created by inducing a linear frequency chirp onto one of two near counter-propagating laser beams which interfere to create the moving lattice beams. A simulation of this process for molecular hydrogen is shown in Fig. 7. In this simulation we follow the trajectories of 20000 particles placed within a decelerating lattice with a constant chirp over 150 ns and a frequency excursion of 1.1 GHz. We assume a translational gas temperature of H_2 at 1 K seeded in a buffer gas of argon.

To undertake these experiments we have constructed an amplified laser system operating at a wavelength of 1064 nm. This system is largely constructed from conventional commercial nanosecond laser components but, is configured for chirped optical Stark deceleration. This system produces two output beams which can be used to form a constantly decelerated lattice over a timescale from 100 ns to a few microseconds. The laser and amplifier system that we have constructed to accomplish this task is shown schematically in Fig. 8. The amplifier is custom made by Continuum lasers and consists of two, separate amplifier arms each with three 100 mm long Nd:YAG amplifier rods that are flash lamp pumped. One arm is used to produce a constant frequency beam and the other arm for the chirped beam. The flash lamp pumped amplifiers are well established nanosecond Nd:YAG laser technology which are typically used in commercial Q-Switched Nd:YAG laser systems.[42] The unique feature of this system is that the two arms amplify two CW laser beams producing a flat-top temporal profile of constant laser intensity over most of the pulse duration. As the amplifier gain is non-linear as a function of time, the flat-top intensity profile is created by continuously varying the input laser intensity to produce a flat top profile after amplification. This is accomplished using an electro-optic attenuator consisting of a Pockels cell and a polarizer. The required input temporal profile to produce the flat-top is found for a particular pulse energy and length by trial and error. The CW laser input intensity can be modulated by up to 100% in increments of 7 ns for a total duration of 10 microseconds and a flat profile with variations of the order of 5% can be achieved. The CW laser system that is amplified in each arm is produced by a home built continuous wave (CW) Nd:YVO_4 laser which is similar in design to Li *et al.*[43] and produces a narrow line width (<1 MHz) which can also be rapidly tuned (chirped) in frequency. The CW laser system consists of an optical cavity consisting of a 5 mm thick Nd:YVO_4 crystal (doping of 3% atm) which forms the gain medium, as well as the highly reflecting back mirror. An intracavity electro-optical $LiTaO_3$ crystal is used to rapidly tune the laser and an output coupler with a reflectivity of 96% at 1064 nm. The physical

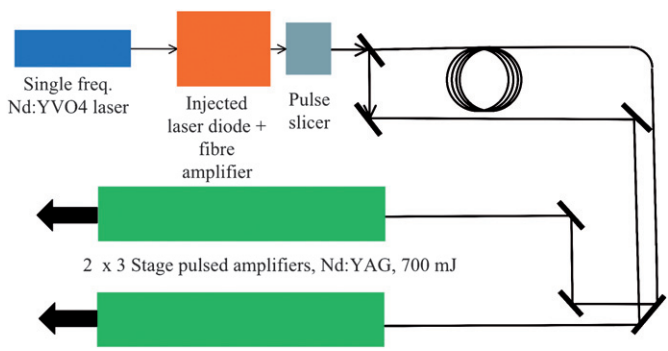

Fig. 8 Schematic diagram of the chirped optical Stark deceleration system which amplifies the output from a Nd:YVO_4 laser up to 700 mJ in each arm over a 1 μs interval.

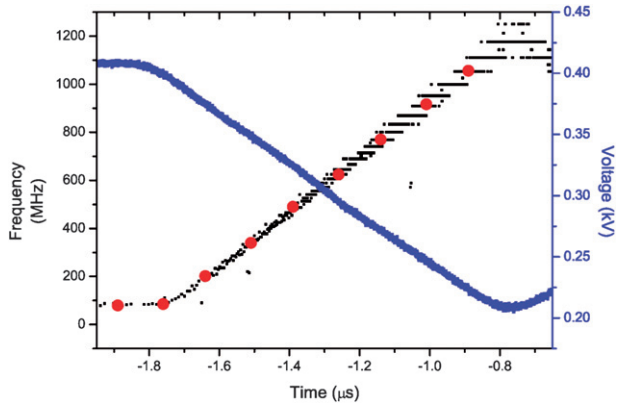

Fig. 9 Frequency of the microchip laser measured as a function of time by heterodyning a fixed frequency laser demonstrating the greater than 1 GHz μs^{-1} frequency chirp required for deceleration experiments.

length of this cavity is approximately 5 mm and is dominated by the 5 mm long by 1 mm thick y-cut electro-optic crystal. A voltage is applied across the 1 mm thick section to modulate the cavity length and thus the frequency of the laser. The Nd:YVO_4 laser crystal is anti-reflection (AR) coated for the 808 nm diode pump laser light and has a highly reflecting coating for the 1064 nm. The laser is pumped by an 808 nm laser diode. This Nd:YVO_4 laser can be linearly frequency chirped over timescales of less than 100 ns with a frequency change per volt of 7 MHz V^{-1}. The laser is maintained to within a few mK to ensure frequency stability. Deceleration experiments typically require frequency excursions of up 1 GHz and this requires a linear voltage ramp of 160 volts over the duration of the deceleration period, which is provided by amplification of a standard laboratory signal generator.

Fig. 9 is a graph of the instantaneous frequency of this laser system over approximately 1 μs. In order to create the chirped and unchirped laser beams for amplification to the energies (>400 mJ) required for deceleration, we firstly amplify the low power beam from the Nd:YVO_4 laser from approximately 10 mW up to 60 mW by injecting this light into a conventional InGaAs Fabry–Perot laser diode operating at 1064 nm.[44] Importantly, this step also serves to reduce intensity variations in the beam introduced by the chirping process. This beam is further amplified in a commercial 1 W Yb fibre amplifier (IPG Photonics). Finally, the preamplified CW beam is subsequently split into two beams of approximately equal intensity by a 50/50 beamsplitter. As the CW beam is unchirped most of the time the chirped temporal component can be superimposed in time with an unchirped component of the beam by sending one of the split beams into a delay line formed by a single mode optical fibre. When both the chirped and unchirped components are temporally co-incident they are subsequently directed into the separate amplifier arms described above to produce the final energies required for deceleration. We are now beginning experiments to utilise this laser system for chirped deceleration experiments and first plan to use this system to decelerate molecular hydrogen into the optical trap described above. We stress that this system is, in principle, capable of decelerating any molecular or indeed any atomic species introduced into the molecular beam, albeit with a different efficiency due to differences in the polarizability and mass.

5 Summary and conclusions

We have outlined a general scheme for cooling molecules to μK temperatures using sympathetic cooling within a deep optical trap and have applied this to the case of sympathetic cooling of H_2. The combination of optical trapping and the use of

ultracold rare gas species is general in principle, and allows the trapping of essentially any species. It also has the potential to mitigate trap losses due to inelastic collisions and also reduces the potential for reactions between many ultracold atomic and molecular species. In addition, the deep optical trap produces high trap oscillation frequencies which help to reduce thermalisation times for species with very different initial temperatures. Such a method also appears to be particularly promising for optical Stark deceleration because the dimensions of the optical trap match well to those of the focused beams used in optical Stark deceleration. We have presented recent developments in the optical Stark deceleration method. This includes the measurement of the role of molecular alignment on the optical dipole force, where we have shown by variation of the polarization that continuous tuning of the well depth of an optical Stark decelerator is possible by changing from linear to circular polarization at a fixed intensity. Finally, we have also described a laser and amplifier system that has been constructed for chirped optical Stark deceleration experiments and have shown that it appears capable of decelerating a range of molecular species, including molecular hydrogen, with a narrow energy spread which can be used for future sympathetic cooling experiments and collision studies.

References

1 S. Chu, L. Hollberg, J. Bjorkholm, A. Cable and A. Ashkin, *Phys. Rev. Lett.*, 1985, **55**, 48.
2 T. Köhler, K. Góral and P. Julienne, *Rev. Mod. Phys.*, 2006, **78**, 1311–1361.
3 K. Jones, E. Tiesinga, P. Lett and P. Julienne, *Rev. Mod. Phys.*, 2006, **78**, 483–535.
4 J. D. Weinstein, R. deCarvalho, T. Guillet, B. Friedrich and J. M. Doyle, *Nature*, 1998, **395**, 148.
5 H. L. Bethlem, A. J. A. van Roij, R. T. Jongma and G. Meijer, *Phys. Rev. Lett.*, 2002, **88**, 133033.
6 N. Vanhaecke, U. Meier, M. Andrist, B. H. Meier and F. Merkt, *Phys. Rev. A*, 2007, **75**(3), 031402.
7 J. Gilijamse, S. Hoekstra, S. van de Meerakker, G. Groenenboom and G. Meijer, *Science*, 2006, **313**, 1617–1620.
8 E. R. Hudson, H. J. Lewandowski, B. C. Sawyer and J. Ye, *Phys. Rev. Lett.*, 2006, **96**, 143004.
9 M. Gangl and H. Ritsch, *Phys. Rev. A*, 2001, **64**, 063414.
10 A. Mosk, S. Kraft, M. Mudrich, K. Singer, W. Wohlleben, R. Grimm and M. Weidemuller, *Appl. Phys. B*, 2001, **73**, 791.
11 M. Lara, J. L. Bohn, D. Potter, P. Soldan and J. M. Hutson, *Phys. Rev. Lett.*, 2006, **97**, 183201.
12 P. Soldan and J. M. Hutson, *Phys. Rev. Lett.*, 2004, **92**, 163202.
13 A. Aspect, E. Arimondo, R. Kaiser, N. Vansteenkiste and C. C. Tannoudji, *Phys. Rev. Lett.*, 1988, **61**, 826.
14 F. Shimizu, K. Shimizu and H. Takuma, *Phys. Rev. A*, 1989, **39**, 2758.
15 H. Katori and F. Shimizu, *Jpn. J. Appl. Phys.*, 1990, **29**, L2124.
16 C. Y. Chen, Y. M. Li, K. Bailey, T. P. O'Connor, L. Young and Z. Lu, *Science*, 1999, **286**, 1139.
17 M. Walhout, H. J. L. Megens, A. Witte and S. L. Rolston, *Phys. Rev. A*, 1993, **48**, R879.
18 R. D. Knight and L. Wang, *Phys. Rev. A*, 1985, **32**(5), 2751.
19 T. Takekoshi, J. R. Yeh and R. J. Knize, *Opt. Commun.*, 1995, **114**, 421.
20 A. Mosk, S. Jochim, H. Moritz, T. Elsasser, M. Weidemller and R. Grimm, *Opt. Lett.*, 2001, **26**, 1837.
21 S. K. Lee, H. S. Lee, J. M. Kim and D. Cho, *J. Phys. B: At., Mol. Opt. Phys.*, 2005, **38**, 1381.
22 L. S. Cruz, M. Sereno and F. C. Cruz, *Opt. Express*, 2008, **16**, 2909.
23 L. S. Meng, J. K. Brasseur and D. K. Neumann, *Opt. Express*, 2005, **13**, 10085.
24 R. W. P. Drever, J. L. Hall, F. V. Kowalski, J. Hough, G. M. Ford, A. J. Munley and H. Ward, *Appl. Phys. B.*, 1983, **31**, 97.
25 E. D. Black, *Am. J. Phys.*, 2001, **69**, 79.
26 R. Fulton, A. I. Bishop and P. F. Barker, *Phys. Rev. Lett.*, 2004, **93**(24), 243004.
27 R. Fulton, A. I. Bishop, M. N. Shneider and P. F. Barker, *Nat. Phys.*, 2006, **2**, 465.
28 J. C. Flasher and R. C. Forrey, *Phys. Rev. A*, 2002, **65**, 032710.
29 A. Mack, T. K. Clark, R. C. Forrey, N. Balakrishnan, T.-G. Lee and P. C. Stancil, *Phys. Rev. A*, 2006, **74**, 052718.
30 P. Barletta, J. Tennyson and P. F. Barker, *Phys. Rev. A*, 2008, **78**, 052707.

31 P. Barletta, *Eur. Phys. J. D*, 2009, **53**, 33.
32 F. A. Gianturco, T. González-Lezana, G. Delgado-Barrio and P. Villareal, *J. Chem. Phys.*, 2005, **122**, 084308.
33 A. Kalinin, O. Kornilov, L. Yu Rusin and J. P. Toennies, *J. Chem. Phys.*, 2004, **121**, 625–627.
34 H. Sakai, A. Tarasevitch, J. Danilov, H. Stapelfeldt, R. W. Yip, C. Ellert, E. Constant and P. B. Corkum, *Phys. Rev. A*, 1998, **57**, 2794.
35 R. Fulton, A. Bishop and P. F. Barker, *Phys Rev. Lett.*, 2004, **93**, 243004.
36 T. Seideman, *J. Chem. Phys.*, 1997, **107**, 10420.
37 J. Ortigoso, M. Rodriguez, M. Gupta and B. Friedrich, *J. Chem. Phys.*, 1999, **110**, 3870.
38 E. Hamilton, T. Seideman, T. Ejdrup, M. D. Poulsen, C. Z. Bisgard, S. S. Viftrup and H. Stapelfeld, *Phys. Rev. A*, 2005, **72**, 043402.
39 J. Baker, M. Konstantaki and S. Couris, *J. Chem. Phys.*, 1995, **103**, 2436.
40 R. A. Morgan, M. A. Baldwin, A. J. Orr-Ewing, M. N. R. Ashfold, W. J. Burma, J. B. Milan and C. A. de Lange, *J. Chem. Phys.*, 1996, **104**, 6117.
41 P. Barker and M. N. Shneider, *Phys. Rev. A*, 2002, **66**, 065402.
42 A. Seigman, *Lasers*, University Science Books, New York, NY, 1986.
43 Y. Li, A. Viera, S. M. Goldwasser and P. Herczfeld, *IEEE Trans. Microwave Theory Tech.*, 2001, **49**, 2048.
44 M. J. Wright, P. L. Gould and S. D. Gensemer, *Rev. Sci. Instrum.*, 2004, **75**, 4718.

